University of New Orleans
ScholarWorks@UNO

Chemistry Faculty Publications | Department of Chemistry

2011

# Highly Ordered Transition Metal Ferrite Nanotube Arrays Synthesized by Template-Assisted Liquid Phase Deposition

Amin Yourdkhani
*University of New Orleans*, ayourdkh@uno.edu

Gabriel Caruntu
*University of New Orleans*, gcaruntu@uno.edu

Follow this and additional works at: https://scholarworks.uno.edu/chem_facpubs

 Part of the Chemistry Commons

## Recommended Citation
J. Mater. Chem., 2011, 21, 7145

This Article is brought to you for free and open access by the Department of Chemistry at ScholarWorks@UNO. It has been accepted for inclusion in Chemistry Faculty Publications by an authorized administrator of ScholarWorks@UNO. For more information, please contact scholarworks@uno.edu.

View Article Online / Journal Homepage / Table of Contents for this issue
Dynamic Article Links

Journal of Materials Chemistry

Cite this: *J. Mater. Chem.*, 2011, **21**, 7145

www.rsc.org/materials

**PAPER**

# Highly ordered transition metal ferrite nanotube arrays synthesized by template-assisted liquid phase deposition

**Amin Yourdkhani and Gabriel Caruntu***

***Received 19th December 2010, Accepted 1st March 2011***
**DOI: 10.1039/c0jm04441e**

Published on 04 April 2011 on http://pubs.rsc.org | doi:10.1039/C0JM04441E
Downloaded by UNIVERSITY OF NEW ORLEANS on 05 March 2013

Highly ordered spinel ferrite $M_xFe_{3-x}O_4$ (M = Ni, Co, Zn) nanotube arrays were synthesized in anodic aluminium oxide (AAO) templates with a pore size of 200 nm by combining a liquid phase deposition (LPD) method with a template-assisted route. The morphology of the transition metal ferrite nanotubes was characterized by electron microscopy (FE-SEM; TEM, SAED and HRTEM) and atomic force microscopy (AFM), whereas their chemical composition was determined by inductive coupling plasma (ICP). The phase purity was studied by X-ray diffraction (XRD) and the magnetic properties of the nanotubes were measured by SQUID measurements. Unlike the deposition of thin film structures, nanotube arrays form within the pores of the AAO templates in a much shorter time due to the attractive interactions between the positively charged AAO and the negatively charged metal complex species formed in the treatment solution. The as-deposited nanotubes are amorphous in nature and can be converted into polycrystalline metal ferrites *via* a post-synthesis heat treatment which induce the dehydroxylation, crystallization and formation of the spinel structure. The resulting nanotubes are uniform with smooth surfaces and open ends and their wall thickness can be varied from 4 to 26 nm by increasing the deposition time from 1 to 4 h. Significant differences in the magnetic properties of the ferrite nanotubes have been observed and these differences seem to result from the chemical composition, the wall thickness and the annealing temperature of the spinel ferrite nanotubes.

## 1. Introduction

Nanotubular architectures of metal oxides have attracted a growing interest due to their unique size and shape-dependent properties which find potential applications in highly efficient selective catalysis,[1–3] chemical and biological sensing,[4–6] photonics,[7] pollutants decomposition,[8,9] generation of hydrogen fuel,[10,11] energy conversion and storage[12–14] and biotechnology.[15,16] In particular, one-dimensional magnetic nanostructures are very promising for the design of ultrahigh density magnetic storage media since they exhibit a structural anisotropy resulting from the nanoscale confinement in two-dimensions.[17] With the increasing trend towards miniaturization in computing and data storage, the natural tendency to achieve high areal densities in magnetic storage media consists of reducing the bit size and increasing the number of magnetic grains. However, down scaling the individual magnetic grains is limited by the disappearance of the magnetic order in 0-D magnetic structures below a critical size. This phenomenon, known as the superparamagnetic limit is the result of the thermal fluctuations which become comparable to the energy associated with the magnetic phase transition as the size of the nanoparticles is decreased below a threshold value characteristic to each magnetic material.[18,19] This thermally activated magnetization reversal can be alleviated by replacing the 0-D nanostructures (nanodots and spherical nanoparticles) with regular arrays of 1-D nanostructures (nanowires, nanotubes, nanorods or nanobelts) which are magnetic due to their enhanced magnetic anisotropy, thereby extending the storage densities beyond the superparamagnetic limit.

Among the metal oxides, spinel ferrites $MFe_2O_4$ have a particular technological relevance due to their relatively easy and low cost synthesis, high chemical stability and mechanical hardness coupled with the wide range of tunable magnetic properties by simply changing the ratio and the chemical identity of the metal ions.[20–24] In addition, nanotubular iron oxide nanostructures are biocompatible, have porosity and can float in fluids along with large, distinct inner and outer surfaces which enable the capture, concentration and encapsulation of different chemical and biological species being attractive as magnetic vectors in cell targeting and drug delivery,[15,25–27] molecular and bio-separation[28,29] and contrast agents in magnetic resonance imaging. Despite their unique physical and morphological properties and the wide range of potential technological applications, the synthesis of high quality transition metal ferrite nanotubular structures still remains a sparsely investigated area. Spinel ferrite nanotubes are conventionally prepared by template-assisted methods in which hollow 1-D structures are formed in the space confined within the

*Advanced Materials Research Institute, University of New Orleans, New Orleans, LA, USA*

Published on 04 April 2011 on http://pubs.rsc.org | doi:10.1039/C0JM04441E
Downloaded by UNIVERSITY OF NEW ORLEANS on 05 March 2013

pores of a template by electrodeposition of the metals followed by oxidation,[30,31] sol–gel,[32,33] thermal decomposition[34] or chemical vapor deposition.[35] Anodic aluminium oxide (AAO) or carbon nanotubes[36] have been used as templates and since the resulting nanotubes are usually amorphous a post-synthesis heat treatment step is needed in order to ensure the crystallization of the desired oxide. Upon the subsequent removal of the template the nanotubes can be liberated; however, in most cases are not free-standing, due to their high aspect ratio which reproduces the thickness and the pore diameter of the template.

A simple, environmentally benign and easily scalable method for the chemical deposition of thin film structures is the so-called liquid phase deposition (LPD). This approach is based on slow hydrolysis of supersaturated solutions of metal fluoro-complexes at low temperature whereby the fluoride ions in the inner coordination sphere of the metal are progressively replaced by $OH^-$ ions and/or water molecules:

$$MF_n^{(n-2m)-} + mH_2O \rightleftharpoons MO_m + nF^- + 2mH^+ \quad (1)$$

$$H_3BO_3 + 4HF^- \rightleftharpoons BF_4^- + H_3O^+ + 2H_2O \quad (2)$$

Since the hydrolysis occurs *via* an equilibrium reaction, the formation of the metal oxide can be accelerated by adding a fluoride scavenger such as $H_3BO_3$ which captures the $F^-$ ions forming water soluble complexes which can be easily removed from the solution. This method was initially developed for the deposition of thin films of binary oxides being extended to the preparation of nanotubes of binary oxides and core–shell nanotubular architectures such as $TiO_2$[37,38] and $CdS@TiO_2$.[39] Recently, Hsu and coworkers extended this approach to the synthesis of multicomponent oxide nanotubes, such as perovskite titanates $ABO_3$ (A = Ba and Pb),[40,41] whereas our research group developed a LPD-based synthetic methodology for the fabrication of highly uniform transition metal ferrite films,[42,43] as well as magnetoelectric bilayered structures, respectively.[44]

In this work we describe the first synthesis of transition metal ferrite $M_xFe_{3-x}O_4$ (M = Co, Ni, Zn) tubular nanostructures with controlled diameter and wall thickness by using a template-assisted liquid phase deposition (LPD) method. The ferrite nanotubes were obtained under nearly ambient conditions using anodic aluminium oxide (AAO) membranes with a pore of 200 nm as templates. These nanotubes can be used as templates for the design of tubular core–shell spinel–perovskite nanocomposites which can potentially exhibit an enhanced magnetoelectric effect as a result of the high interfacial coupling between the two constituent phases.

## 2. Experimental procedure

The synthesis of spinel ferrite nanotubular structures was performed in open atmosphere by using a magnetic hotplate (IKA Works, Inc.) equipped with a temperature controller and a pH electrode. Ordered arrays of ferrite nanotubes were fabricated from treatment solutions obtained by mixing a solution containing 0.25 g FeOOH dissolved in 50 ml of a 1 M $NH_4 \cdot HF$ solution with a homogeneous 2.22 M solution of a transition metal nitrate $M(NO_3)_2$ (M = Co, Ni, Zn) and 40 ml of 0.5 M boric acid solution used as a fluoride scavenger.[42] The treatment solutions were prepared by dissolving reagent grade purity chemicals (Alfa Aesar) in deionized water (18 MΩ) obtained from a Barnstead Nanopure water purification system. These initial solutions were clear and retained the color of the transition metal nitrate salt without the formation of precipitates at room temperature. Prior to each experiment, Whatman Anodisc anodized aluminium oxide (AAO) templates with a thickness of 60 μm and a pore diameter of 200 nm were immersed vertically in the solution and maintained at 45 °C for different time periods. During deposition the color of the AAO templates changed progressively from white color to brown. At the end of the deposition process the templates were removed from the solution, rinsed carefully with deionized water and dried at room temperature for 3 hours. Samples were subsequently annealed at temperatures 750 °C for 6 hours to promote the dehydroxylation and dehydration reactions and to yield the corresponding crystalline spinel ferrite nanotubes. After the formation of the metal oxide nanotubes, the superficial metal oxide layer formed templates each side of the template was mechanically polished followed by the removal of the membrane upon immersion in a 6 M sodium hydroxide solution for 30 min, followed by washing and centrifugation in water. The resulting spinel ferrite nanotube powders were dried under vacuum for 8 h at room temperature then stored and subjected to structural characterization and the measurement of the magnetic properties.

## 3. Characterization of the spinel ferrite nanotube arrays

The identification of the crystalline phases was performed by X-ray diffraction using a Philips X'Pert system equipped with a curved graphite single-crystal monochromator (CuK$\alpha$ radiation; $\lambda$ = 0.1541778 nm at 40 mA and 40 kV). Chemical composition of fabricated nanotubes was determined by inductive coupled plasma (ICP) spectroscopy, model Varian FT220S flame absorption spectrometer. Field-emission scanning electron microscopy experiments (FE-SEM) were performed with a LEO 1530VP instrument with an accelerating voltage of 200 kV for the study of the structure, surface topology and the morphological characteristics of metal oxide nanotubes. Atomic force (AFM) and magnetic force (MFM) microscopy images of the ordered nanotube arrays of spinel ferrites were collected with an MFP-3D-SA Asylum Research Atomic Force Microscope (AFM). MFM tips with field strength of ~10 Oe with a vertical magnetization were used to image individual ferrite nanotubes placed horizontally on a non-magnetic substrate. Temperature dependent measurements of the magnetization of the nanotubes immobilized within the pores of the AAO templates were performed with a superconducting quantum interference device (SQUID), model Quantum Design MPMS-7XL, in the range from 5 to 300 K by applying a static magnetic field up to 6 Tesla.

## 4. Results and discussion

### (a) Mechanism of formation of the spinel ferrite nanotubular structures

Similar to the methodology that we developed previously for the deposition of mirror-like ferrite thin films,[42,43] nanotubular

 This journal is © The Royal Society of Chemistry 2011

Published on 04 April 2011 on http://pubs.rsc.org | doi:10.1039/C0JM04441E
Downloaded by UNIVERSITY OF NEW ORLEANS on 05 March 2013

structures were synthesized method at temperatures as low as 45 °C. The pH of the initial solutions ranged between 4.8 and 5.5 and progressively decreased to values between 3.9 and 4.4 at the end of the deposition process. It is worth mentioning that the formation of spinel ferrite nanotubes by the proposed template-assisted route occurs much faster than that conventional liquid phase deposition of thin film structures. Specifically, during the deposition of thin film structures turbidity is observed in the treatment solution maintained at 45 °C only after 3.5–4 h and the deposition of the films is complete after 1–2 more additional hours after the solution turned cloudy. Unlike the thin film structures, under similar conditions a change in color of the AAO template is observed after 15–30 min after its immersion in the treatment solution indicating the formation of spinel ferrite nanotubes which can increase the thickness of their walls while maintained in solution up to 4–5 h, eventually leading to the formation of nanowires, depending on the concentration of the metal precursors in solution. Generally, the deposition of metal oxide nanostructures by the LPD method is considered to take place by a two-step mechanism. While in the first step the metal fluoro-complexes formed in solution undergo a slow hydrolysis process generating metal oxides, hydroxides and oxyhydroxides, in the second step these intermediates are heat-treated at temperatures typically above 450 °C, thereby yielding the desired metal oxide nanostructures.

Chen and coworkers suggested that during the deposition of perovskite-type $ATiO_3$ nanotubes (A = Ba, Sr) by a template-assisted LPD route the metal clusters, which are negatively charged attach onto the walls of the positively charged pores of the alumina template.[40] This assumption was based on the value of the isoelectric point of alumina, according to which the surface of alumina has no electrical charges at pH values between 8 and 9 whereas in acidic solutions, which are conventionally used in the deposition of metal oxides by the liquid phase deposition method[45–47] the alumina surface is positively charged. To confirm the validity of this hypothesis, a control experiment was performed by immersing an AAO membrane, a microscope slide and a 1 $cm^2$ piece of (100) silicon into a solution containing stoichiometric amounts of $Fe^{3+}$ and $Co^{2+}$ ions, $NH_4F.HF$ and boric acid. The treatment solution was subsequently heated to 45 °C. After 30 min, at this temperature the membrane gradually changed its color from white to light brown, whereas no deposition of thin films was noticed onto the glass and silicon substrates. As the hydrolysis reaction progressed, the color of the membrane darkened and the formation of a thin film structure was noticed on the planar substrates. These observations confirm that the fast deposition of the spinel ferrite nanotubular structures in the presence of AAO templates is the result of the electrostatic attractions between the positive charges induced on the surface of the alumina and the negatively charged complex ions generated in the treatment solution. A schematic of the deposition process is shown in Fig. 1.

When the treatment solution penetrates the pores of the membrane, the negatively charged species from the solution are attracted by the positively charged surfaces of the membrane. As the concentration of the negative charge metal fluoro-complex within the pores of the membrane increases, they accumulate along the inner walls whereby they undergo a slow hydrolysis leading to the preferential growth of metal oxide/hydroxide or oxyhydroxide species along the pore wall, thereby producing nanotubular structures.

### (b) Structural and morphological characteristics of the transition metal ferrite nanotubes

The room temperature crystal structure of the transition metal ferrite nanotubes was investigated by powder X-ray diffraction (PXRD). As seen in Fig. 2, the ferrite nanotubes obtained after the heat treatment at 750 °C are crystalline and free of impurities phases such as $Fe_2O_3$ or MO (M = Co, Ni, Zn) oxides. All the reflection peaks in the XRD pattern of the ferrite nanotubes can be readily indexed into a cubic unit cell (space group *Fd3m*) and the refined lattice constants of 8.33(1) Å, 8.274(2) Å and 8.32(7) Å for the Co-ferrite, nickel ferrite and the Zn-ferrite, respectively.

The intensity of the reflections of the nanotube powdered samples is lower than that corresponding to the bulk phase whereas the peaks are broadened due to the small size of the crystalline domains diffracting coherently the X-ray radiation. For the cobalt ferrite nanotubes samples the average grain size calculated by using the Scherer's formula[48] was 11 nm for the nanotubes obtained after 1 h and increased to 17 and 24 nm for ferrite nanotubes obtained after 2 h and 4 h, respectively. The apparent asymmetry and broadening of the peaks in the XRD pattern of the zinc ferrite nanotubes is presumably due to the lower crystallinity of the sample associated with a smaller size of the crystallites as compared to those of the other ferrite nanotubes (7.8 nm).

The composition of the ferrite nanotubes separated from the AAO membranes was determined by ICP combined with EDX analysis. The values of the M/Fe molar ratios determined by ICP analysis were 0.32/2.68; 0.66/2.34 and 1.5/1.5 for the $MFe_{3-x}O_4$ (M = Co, Ni and Zn), respectively. Although in this paper we describe the synthesis of transition metal ferrite nanotubes with the particular chemical compositions indicated above, as it has been documented in the case of ferrite films obtained by the LPD method, the composition of the nanostructured spinel ferrites can be varied in a wide range by simply adjusting the molar ratio between the metal and the $Fe^{3+}$ in the treatment solution, which also allows for a fine control of their magnetic properties.[42] The FE-SEM micrographs of the ferrite nanotubular architectures after the heat treatment at 750 °C are presented in Fig. 3(a)–(i). Except for Fig. 3(h), which shows Zn-ferrite nanotubes immobilized within the pores of the AAO membrane, all the other figures show freestanding ferrite nanotubes obtained after the removal of the AAO templates in a 6 M NaOH solution followed by the washing and drying of the nanopowders. Prior to the removal of the membranes, their surfaces were cleaned by mechanical polishing in order to eliminate the superficial metal oxide layer formed during the deposition. All nanotubes are open-ended; they have smooth and uniform surfaces and free of defects, such as cracks or holes. The observed filling rate is 100% indicating that the ferrite nanotubular structures form *via* a homogeneous growth mechanism. The length of the nanotubes is 60 μm whereas the average outer diameter is 200 nm, values which are comparable to the physical dimensions of the AAO templates. One of the main advantages of the LPD method as compared by the other chemical methods used in the

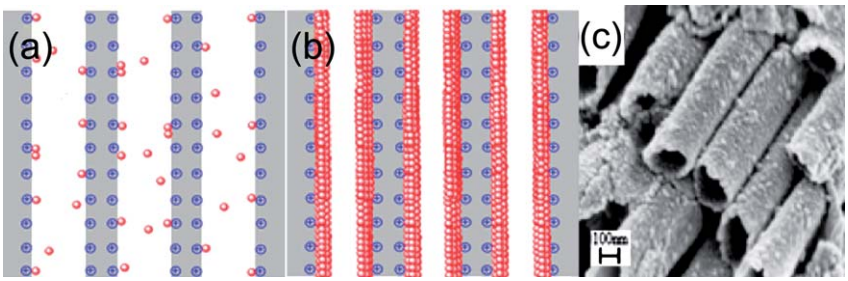


**Fig. 1** Schematic of the mechanism of formation of spinel ferrite nanotubular architectures by the attachment and immobilization of the negatively charged metal clusters onto the inner walls of the positively charged AAO membranes (a and b); (c) a typical FE-SEM image of nanoparticulate nanotubes.

Published on 04 April 2011 on http://pubs.rsc.org | doi:10.1039/C0JM04441E
Downloaded by UNIVERSITY OF NEW ORLEANS on 05 March 2013

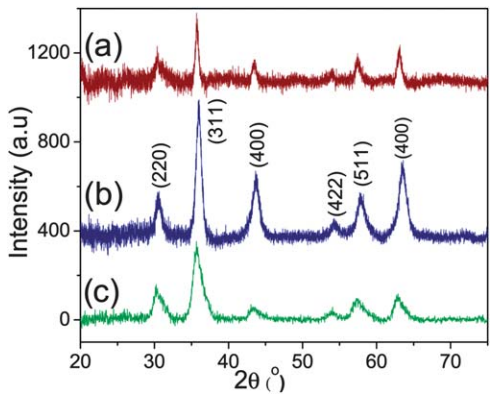


**Fig. 2** XRD patterns of Co (a); Ni (b) and Zn (c) ferrite nanotubes annealed at 750 °C for 6 h.

template-assisted synthesis of ferrite tubular nanostructures is that the hydrolysis reactions are performed in solutions with a pH typically higher than 3.5 which prevents the etching of the AAO templates or increase the pore sizes as it was reported previously in the case of other template-assisted solution-mediated methods for the synthesis of tubular nanostructures.[39] The FE-SEM micrographs also reveal the influence of the sonication process on the orientation of the nanotubes, while the Co-ferrite nanotubes obtained by sonicating the sample during the removal of the AAO template are oriented in random directions (Fig. 3(a)), in the case when no sonication was used to remove the template, highly aligned nanotube arrays were obtained.

In Fig. 4 is presented the mass loss profile of a sample collected by scratching the film formed after the deposition of the $Co_{0.32}Fe_{2.68}O_4$ nanotubes and then subjected to a thermal

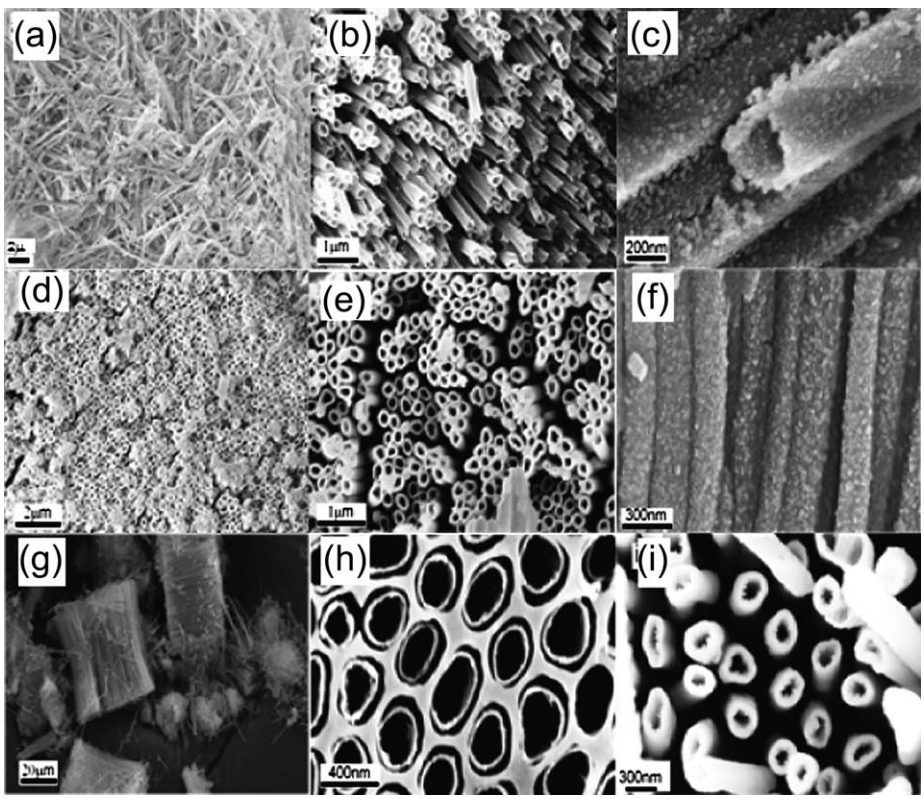


**Fig. 3** Top and side view FE-SEM micrographs of Co-ferrite (a–c), Ni-ferrite (d–f) and Zn-ferrite (g–i) nanotubes with a diameter of 200 nm.

 This journal is © The Royal Society of Chemistry 2011

Published on 04 April 2011 on http://pubs.rsc.org | doi:10.1039/C0JM04441E
Downloaded by UNIVERSITY OF NEW ORLEANS on 05 March 2013

treatment in the temperature range from 25 to 700 °C under flowing $N_2$. The TGA curve exhibits a very well-defined decrease in the mass of the sample with two inflection points. While the first inflection point appears at 88 °C and corresponds to the elimination of the hydrated water molecules (~17.08% mass loss), the second appears at 241 °C and is associated with the elimination of lattice water molecules in tandem with dehydroxylation and condensation reactions of the metal hydroxides and oxyhydroxides (~30.16% mass loss) eventually yielding the corresponding spinel ferrite. These thermal events are also observed in the DSC curve which exhibits five well defined endothermic peaks at 43, 68, 189, 272 and 692 °C which are indicative of the transition from the metal hydroxide precursors to the spinel ferrite structure. In general, in conventional template-assisted sol–gel approaches metal oxide nanotubes form by the wetting the inner pores of the template with a sol and its subsequent conversion into a gel followed by a heat treatment at high temperature which makes virtually impossible the variation of the wall thickness of the nanotubes.[49–52]

Unlike the sol–gel routes, in the liquid phase deposition method metal oxides with different dimensionality (1-D or 2-D) form by the attachment of fine particles initially formed in solution.[42] Based on the foregoing arguments, it is reasonable to assume that nanotubes initially form near the inner walls of the template and then extend towards the inner volume of the nanopores by the attachment of fine particles initially precipitated in solution.[44] Therefore, when the deposition is performed at a particular temperature, the wall thickness of the metal oxide nanotubes can be controlled by varying the deposition time. In Fig. 5(a)–(c) are presented the TEM images of the individual $Co_{0.32}Fe_{2.68}O_4$ nanotubes with a diameter of 200 nm obtained by soaking the AAO membranes into the treatment solution for different periods of time, that is 1, 2 and 4 hours, respectively. Examination of the TEM micrographs of the Co-ferrite nanotubes presented in Fig. 5(a)–(c) clearly shows that the wall thickness increases from 10 to 16 and 21 nm with increasing the deposition time from 1 to 2 and 4 h, respectively. Moreover, the ferrite nanotubes are uniformly being composed of small, spheroidal particles with an average diameter of 4–5 nm; they possess a straight shape without holes or other defects which are oftentimes observed in oxide nanotubes obtained by sol–gel approaches which form as a result of the so-called Raleigh instabilities.[52]

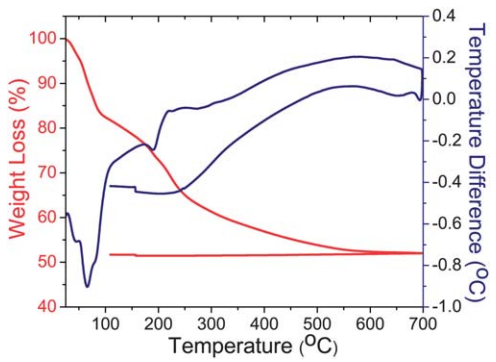


**Fig. 4** TGA and DSC profiles of the as-prepared powder obtained during the synthesis of the $Co_{0.32}Fe_{2.68}O_4$.

Fig. 5(d) represents the SAED image of the individual nanotube presented in Fig. 5(c) which exhibits a series of strong, concentric rings with a spotted appearance, which overlap perfectly the diffraction peaks in the XRD pattern thereby substantiating that the individual ferrite nanotubes are highly crystalline. The zone axis for the SAED image is the {001} crystalline direction. The high crystallinity of the nanotubes was also proved by the HRTEM analysis which suggests that the ferrite nanotubes obtained by this method are smooth and dense. The lattice fringes appearing in Fig. 5(e) correspond to an interplanar distance of 2.93 Å, ascribed to the (222) family of planes of the $CoFe_2O_4$ structure (Fig. 5(e)). A further investigation of the morphology of the individual ferrite nanotubes was performed by atomic force microscopy (AFM). By preparing a diluted solution of ferrite nanotubes and depositing it onto a Si substrate followed by the natural evaporation of the solvent, it is possible to obtain isolated nanotubes which can be probed individually by magnetic force microscopy (MFM). In Fig. 6(a) is shown an AFM image representing two Co-ferrite nanotubes attached together and deposited onto a conductive (100) Si substrate with a native $SiO_2$ layer.

### c) Magnetic properties of transition metal ferrite nanotubes

In Fig. 6(a) and (b) are shown the hysteresis loops of the $Zn_{1.5}Fe_{1.5}O_4$ nanotube arrays measured at room temperature with the magnetic field applied parallel and perpendicular to the long axis of the nanotubes.

The $Zn_{1.5}Fe_{1.5}O_4$ nanotube arrays are saturated at $H_c = 4$ kOe and present coercivity and squareness ($SQ = M_r/M_s$) values which vary from $H_{c\parallel} = 51$ Oe and $SQ_\parallel = 0.047$ to $H_{c\perp} = 56$ Oe and $SQ_\perp = 0.051$ by changing the orientation with respect to the magnetic field. The absence of a noticeable difference in the coercivity values of the sample when its orientation changes from parallel to perpendicular to the magnetic field suggests that the Zn-ferrite nanotubes do not present perpendicular anisotropy and the shape anisotropy contribution is not significant to the total anisotropy of the samples. This may be due to the polycrystalline nature of the nanotubes as well as the small size and random orientation of the constituting grains. This will lead to an irregular distribution of the magnetic spins and was experimentally observed in the case of other ferrite nanotubular structures obtained by solution-based routes such as $\gamma$-$Fe_2O_3$,[53] Co-ferrite[33] or Ni-ferrite nanotubes,[54] respectively. To gain a better insight into the magnetic properties of the Zn-ferrite nanotubes the magnetization of the sample was measured as a function of the temperature in both zero-field-cooling (ZFC) and field-cooling (FC) modes. During these measurements a magnetic field of H = 100 Oe was applied parallel to the long axis of the nanotube arrays and the magnetization of the sample was measured in the temperature range from 5 to 300 K.

As seen in Fig. 6(d), Zn-ferrite nanotubes are superparamagnetic at room temperature and present a maximum in the ZFC curve at $T = 97$ K, which corresponds to the blocking temperature $T_B$. When the sample reaches this temperature the magnetic energy of the Zn-ferrite nanotubes becomes equal to the thermal energy and the orientation of the magnetic spins is randomized by the thermal disorder. This behavior was furthermore confirmed by the measurement of the hysteresis

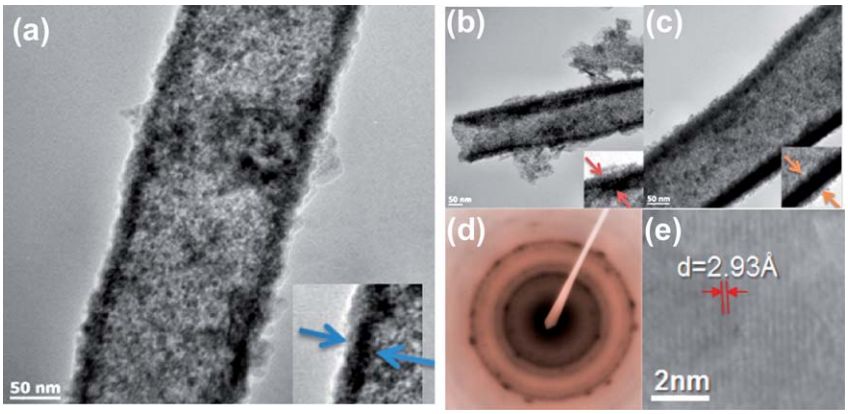


**Fig. 5** TEM images of $Co_{0.32}Fe_{2.68}O_4$ nanotubes with different wall thicknesses fabricated *via* LPD by maintaining the template in the treatment solution for 1 h (a), 2 h (b) and 4 h (c), respectively. (d and e) SAED and HRTEM patterns of a single nanotube.

loops at 5 K (Fig. 6(c)), which clearly indicate a ferrimagnetic behavior of the $Zn_{1.5}Fe_{1.5}O_4$ nanotubes with values of the coercivity of $H_{c\|} = 1.36$ kOe and $H_{c\perp} = 1.17$ kOe, whereas the remanent squareness was $SQ_{\|} = 0.29$ and $SQ_{\perp} = 0.26$, respectively. These results are in agreement with those obtained in the case of spinel ferrite thin film structures obtained by liquid phase deposition which are also constructed by small particles and present a blocking temperature of 108 K.[42–44] Similar to the Zn-ferrite nanotube arrays, the Ni-ferrite nanotubes are superparamagnetic at room temperature, with a blocking temperature of 256 K (ZFC/FC data not shown).The hysteresis loops of the $Ni_{0.66}Fe_{2.34}O_4$ nanotubes measured at room temperature and 5 K with the magnetic field applied parallel to the long axis of the nanotubes are presented in Fig. 7 (a) and (b). The values of the coercivity and squareness increased from $H_{c\|} = 73$ Oe and $SQ_{\|} = 0.065$ at 300 K to $H_{c\|} = 1520$ Oe and $SQ_{\|} = 0.38$ at 5 K, indicating that the $Ni_{0.66}Fe_{2.34}O_4$ nanotubular structures present a magnetic behavior similar to that observed in the case of the Zn-ferrite nanotubes.

In Fig. 8 are shown the magnetization curves of the $Co_{0.32}Fe_{2.68}O_4$ nanotubes with different wall thicknesses deposited by LPD at 45 °C.

After the synthesis, the ferrite nanotubes were subjected to a heat treatment at 750 °C for 6 h under a static atmosphere and the measurement of the magnetic properties was performed with non-interacting nanotubes confined within the channels of the

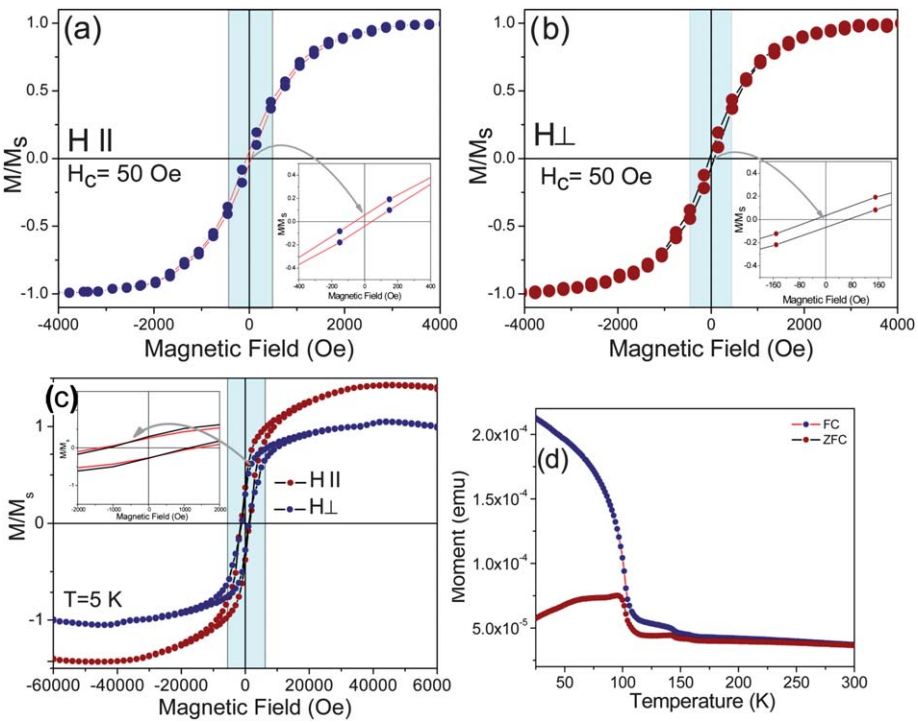


**Fig. 6** Representative room temperature hysteresis loops (a–c) and magnetization *vs.* temperature curves for $Zn_{1.5}Fe_{1.5}O_4$nanotubes (d) with a diameter of 200 nm immobilized within the pores of the AAO membrane. The insets represent an enlarged view of the *M vs. H* curves in the low field region.

 This journal is © The Royal Society of Chemistry 2011

Published on 04 April 2011 on http://pubs.rsc.org | doi:10.1039/C0JM04441E
Downloaded by UNIVERSITY OF NEW ORLEANS on 05 March 2013

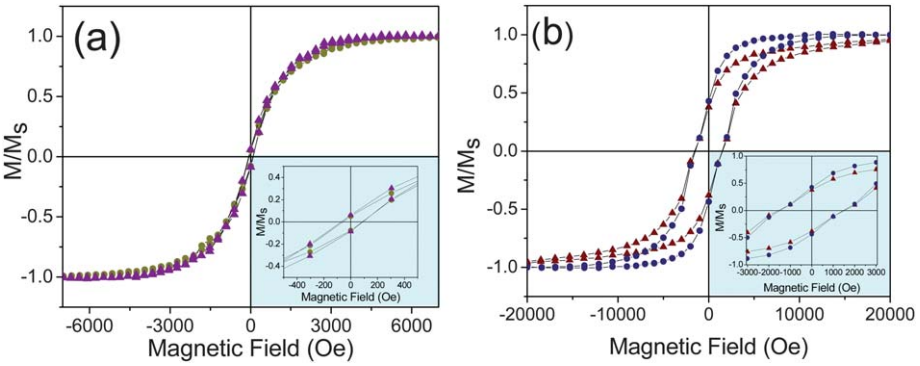


**Fig. 7** *M vs. H* curves at 300 K (a) and 5 K (b) of the $Ni_{0.66}Fe_{2.34}O_4$ nanotubes. Insets represent close-up of the hysteresis loops to indicate their coercivity. The insets represent an enlarged view of the *M vs. H* curves in the low field region.

Published on 04 April 2011 on http://pubs.rsc.org | doi:10.1039/C0JM04441E
Downloaded by UNIVERSITY OF NEW ORLEANS on 05 March 2013

AAO membrane. As seen in Fig. 8 and 9, a high magnetic field does not saturate the magnetization of the nanotube samples; this situation is similar to that reported previously in the case of iron oxide[55] and spinel ferrite[33,54] and can be presumably ascribed to the surface disorder of the magnetic spins in these nanotubular structures. The values of the coercivity and squareness for the $Co_{0.32}Fe_{2.68}O_4$ nanotubes with different wall thicknesses are presented in Table 1. The hysteresis loops become broader with increasing the wall thickness of the Co-ferrite nanotubes which corresponds to a monotonous increase of the coercive field. The remanent squareness of the nanotubes follows a similar pattern, although its variation is not as uniform as that observed for coercivity. Moreover, the values of the remanent squareness were consistently found to be slightly higher in the parallel direction of the nanotubes as compared to those observed for a perpendicular direction, which suggests that the easy axis of the Co-ferrite nanotubes is parallel to the long axis of the nanotubes.

In order to study the influence of the annealing temperature on their magnetic properties, a second series of Co-ferrite nanotube arrays was annealed at 850 °C in air for 6 h. As seen in Fig. 9, the Co-ferrite nanotubes are ferrimagnetic at room temperature and the values of the coercivity are almost three times higher than those of the samples annealed at 750 °C. For example, $H_{c\|} = 288$ Oe for the nanotubes with a wall thickness of 10 nm annealed at 750 °C increases to $H_{c\|} = 958$ Oe after annealing at 850 °C, whereas for the nanotubes with a wall thickness of 21 nm, $H_{c\|}$ increased from 517 Oe to 1450 Oe, respectively. This variation of the coercive field with the annealing temperature in nanotubular structures can be ascribed to the increase of the coercivity of the individual nanoparticles constructing the nanotubes, as a result of the densification and coalescence of the individual grains which eventually lead to an increase of their average diameter.

A detailed characterization of the Co-ferrite nanotubes with different diameters and wall thickness in order to elucidate the mechanism of magnetization reversal is currently underway and will be reported in a forthcoming paper. In summary, we have developed a novel, simple and highly reliable synthetic procedure for the fabrication of transition metal ferrite nanotubular structures that combines a template-assisted route with the liquid phase deposition (LPD) method. Uniform $M_xFe_{3-x}O_4$ (M = Co, Ni, Zn) nanotube arrays with an average diameter of 200 nm were deposited within the pores of AAO templates by the controlled hydrolysis of metal fluoro-complexes at temperatures as low as 45 °C. A subsequent heat treatment at temperatures between 750 and 850 °C in air lead to the formation of the spinel structure from the stoichiometric mixtures of metal hydroxide intermediates. These structures can be obtained as freestanding nanotubes by the selective dissolution of the AAO membrane

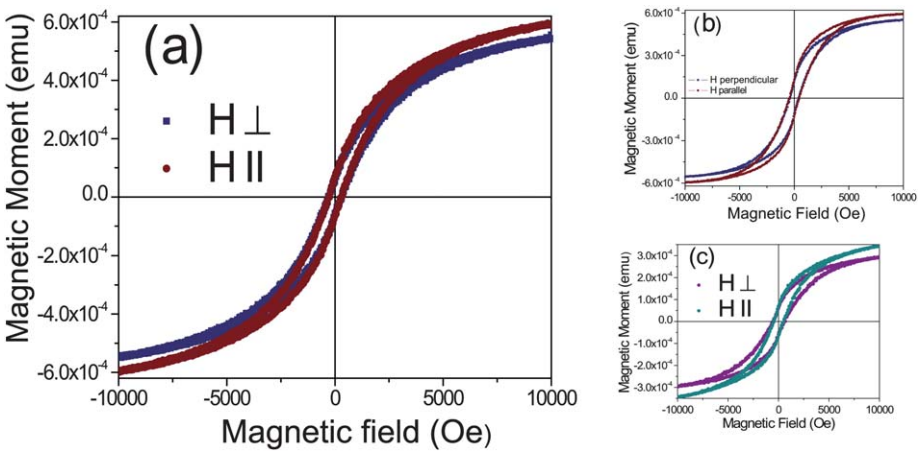


**Fig. 8** Room temperature hysteresis loops of the $Co_{0.32}Fe_{2.68}O_4$ nanotubes with different wall thicknesses (10 (a), 16 (b) and 21 nm (c), respectively). The nanotubular structures were deposited by the LPD method and heat treated at 750 °C for 6 h in air.

Published on 04 April 2011 on http://pubs.rsc.org | doi:10.1039/C0JM04441E
Downloaded by UNIVERSITY OF NEW ORLEANS on 05 March 2013

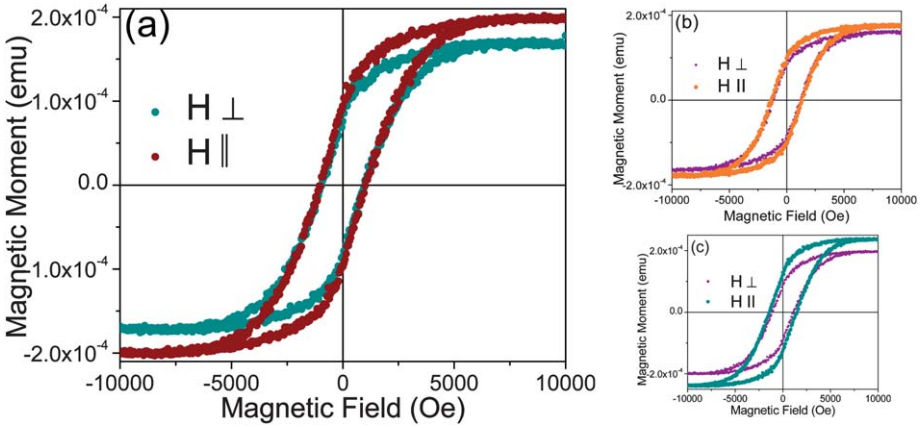


**Fig. 9** Room temperature hysteresis loops of the $Co_{0.32}Fe_{2.68}O_4$ nanotubes with different wall thicknesses (10 (a), 16 (b) and 21 nm (c), respectively). The nanotubular structures were deposited by the LPD method and heat treated at 850 °C for 6 h in air.

**Table 1** The values of the coercivity and remanent squareness of the $Co_{0.32}Fe_{2.68}O_4$ nanotubes with different wall thicknesses obtained at 750 and 850 °C, respectively

| | $H_c$/Oe | | SQ = $M_r/M_s$ | |
|---|---|---|---|---|
| Wall thickness/nm | ∥ | ⊥ | ∥ | ⊥ |
| *Annealed at 750 °C* | | | | |
| 10 | 288 | 308 | 0.11 | 0.09 |
| 16 | 388 | 451 | 0.22 | 0.20 |
| 21 | 517 | 615 | 0.19 | 0.20 |
| *Annealed at 850 °C* | | | | |
| 10 | 958 | 990 | 0.47 | 0.45 |
| 16 | 1332 | 1228 | 0.56 | 0.52 |
| 21 | 1450 | 1148 | 0.54 | 0.45 |

template. The wall thickness of the metal oxide nanotubes can be controlled from 10 to 21 nm by varying the deposition time. Small differences in the coercivity of the ferrite nanotubes were observed when changing their orientation from parallel to perpendicular to the magnetic field, indicating that the magnetocrystalline anisotropy is dominant and the shape anisotropy has a little influence on the magnetic anisotropy. Therefore, unlike the Ni and Zn-ferrite nanotubes, which exhibit a superparamagnetic behavior at room temperature, the Co-ferrite nanotubes are ferrimagnetic and their coercivity increases with increasing the wall thickness and the annealing temperature.

This new process opens up opportunities for the controlled synthesis of ferrite materials with nanotubular geometry, high surface area, controllable morphology and distinct magnetic properties which can be potentially used in different biomedical applications, as well as building blocks for the design of core–shell nanotubular architectures in magnetic data storage and energy conversion applications.

## Acknowledgements

This work was supported by the Department of Defense through the DARPA Grant No. HR 0011-09-0047 and the National Science Foundation, through the Grants No. EPS-1003897 and NSF-DMR-1004869.

## References

1 Z. R. R. Tian, J. A. Voigt, J. Liu, B. McKenzie, M. J. McDermott, M. A. Rodriguez, H. Konishi and H. F. Xu, *Nat. Mater.*, 2003, **2**, 821.
2 A. Kolmakov and M. Moskovits, *Annu. Rev. Mater. Res.*, 2004, **34**, 151.
3 D. V. Bavykin, J. M. Friedrich and F. C. Walsh, *Adv. Mater.*, 2006, **18**, 2807.
4 B. Sljukic, C. E. Banks and R. G. Compton, *Nano Lett.*, 2006, **6**, 1556.
5 C. N. R. Rao and M. Nath, *Dalton Trans.*, 2003, 1.
6 Y. S. Ding, X. F. Shen, S. Gomez, H. Luo, M. Aindow and S. L. Suib, *Adv. Funct. Mater.*, 2006, **16**, 549.
7 O. K. Varghese, M. Paulose and C. A. Grimes, *Nat. Nanotechnol.*, 2009, **4**, 592.
8 X. Quan, S. Yang, X. Ruan and H. Zhao, *Environ. Sci. Technol.*, 2005, **39**, 3770.
9 P. Agarwal, I. Paramasivam, N. K. Shrestha and P. Schmuki, *Chem.–Asian J.*, 2010, **5**, 66.
10 J. H. Park, S. Kim and A. J. Bard, *Nano Lett.*, 2005, **6**, 24.
11 G. K. Mor, K. Shankar, M. Paulose, O. K. Varghese and C. A. Grimes, *Nano Lett.*, 2004, **5**, 191.
12 K. Zhu, N. R. Neale, A. Miedaner and A. J. Frank, *Nano Lett.*, 2006, **7**, 69.
13 F. Sauvage, F. Di Fonzo, A. Li Bassi, C. S. Casari, V. Russo, G. Divitini, C. Ducati, C. E. Bottani, P. Comte and M. Graetzel, *Nano Lett.*, 2010, **10**, 2562.
14 K. Zhu, T. B. Vinzant, N. R. Neale and A. J. Frank, *Nano Lett.*, 2007, **7**, 3739.
15 H. Hillebrenner, F. Buyukserin, J. D. Stewart and C. R. Martin, *Nanomedicine*, 2006, **1**, 39.
16 L. M. Bjursten, L. Rasmusson, S. Oh, G. C. Smith, K. S. Brammer and S. Jin, *J. Biomed. Mater. Res., Part A*, 2010, **92**, 1218.
17 J. Escrig, P. Landeros, D. Altbir, E. E. Vogel and P. Vargas, *J. Magn. Magn. Mater.*, 2007, **308**, 233.
18 D. Weller and A. Moser, *IEEE Trans. Magn.*, 1999, **35**, 4423.
19 D. A. Thompson and J. S. Best, *IBM J. Res. Dev.*, 2000, **44**, 311.
20 S. Sun, H. Zeng, D. B. Robinson, S. Raoux, P. M. Rice, S. X. Wang and G. Li, *J. Am. Chem. Soc.*, 2003, **126**, 273.
21 S. Adireddy, C. K. Lin, V. Palshin, Y. M. Dong, R. Cole and G. Caruntu, *J. Phys. Chem. C*, 2009, **113**, 20800.
22 D. Caruntu, Y. Remond, N. H. Chou, M. J. Jun, G. Caruntu, J. B. He, G. Goloverda, C. O'Connor and V. Kolesnichenko, *Inorg. Chem.*, 2002, **41**, 6137.
23 H. Deng, X. Li, Q. Peng, X. Wang, J. Chen and Y. Li, *Angew. Chem., Int. Ed.*, 2005, **44**, 2782.
24 Y. T. Chong, E. M. Y. Yau, K. Nielsch and J. Bachmann, *Chem. Mater.*, 2010, **22**, 6506.
25 C. R. Martin and P. Kohli, *Nat. Rev. Drug Discovery*, 2003, **2**, 29.
26 H. Hillebrenner, F. Buyukserin, J. D. Stewart and C. R. Martin, *J. Nanosci. Nanotechnol.*, 2007, **7**, 2211.
27 S. J. Son, J. Reichel, B. He, M. Schuchman and S. B. Lee, *J. Am. Chem. Soc.*, 2005, **127**, 7316.

 This journal is © The Royal Society of Chemistry 2011

View Article Online


28 S. B. Lee, D. T. Mitchell, L. Trofin, T. K. Nevanen, H. Soderlund and C. R. Martin, *Science*, 2002, **296**, 2198.
29 M. Lee, T. Kim, C. Bae, H. Shin and J. Kim, *J. Met.*, 2010, **62**, 44.
30 Z. H. Hua, R. S. Chen, C. L. Li, S. G. Yang, M. Lu, B. X. Gu and Y. W. Du, *J. Alloys Compd.*, 2007, **427**, 199.
31 D. Q. Gao, Z. H. Shi, Y. Xu, J. Zhang, G. J. Yang, J. L. Zhang, X. H. Wang and D. S. Xue, *Nanoscale Res. Lett.*, 2010, **5**, 1289.
32 Y. Xu, H. Wei, J. Yao, J. Fu and D. Xue, *Mater. Lett.*, 2008, **62**, 1403.
33 G. B. Ji, H. L. Su, S. L. Tang, Y. W. Du and B. L. Xu, *Chem. Lett.*, 2005, **34**, 86.
34 S. Liu, B. Yue, K. Jiao, Y. Zhou and H. He, *Mater. Lett.*, 2006, **60**, 154.
35 S. Kohli, P. R. McCurdy, D. C. Johnson, J. Das, A. L. Prieto, C. D. Rithner and E. R. Fisher, *J. Phys. Chem. C*, 2010, **114**, 19557–19561.
36 C. Pham-Huu, N. Keller, C. Estournes, G. Ehret, J. M. Greneche and M. J. Ledoux, *Phys. Chem. Chem. Phys.*, 2003, **5**, 3716.
37 J. Wang, Y. Cui, H. Li, Z. Wang, K. Huang and G. Sun, *Res. Chem. Intermed.*, 2010, **36**, 17.
38 Y. Zhang, J. Chen and X. Li, *Catal. Lett.*, 2010, **139**, 129.
39 M. C. Hsu, I. C. Leu, Y. M. Sun and M. H. Hon, *J. Cryst. Growth*, 2005, **285**, 642.
40 Y.-Y. Chen, B.-Y. Yu, J.-H. Wang, R. E. Cochran and J.-J. Shyue, *Inorg. Chem.*, 2008, **48**, 681.
41 M. C. Hsu, Y. M. Sun, I. C. Leu and M. H. Hon, *J. Electrochem. Soc.*, 2006, **153**, F260.
42 G. Caruntu, G. G. Bush and C. J. O'Connor, *J. Mater. Chem.*, 2004, **14**, 2753.
43 G. Caruntu, A. Newell, D. Caruntu and C. J. O'Connor, *J. Alloys Compd.*, 2007, **434**, 637.
44 A. Yourdkhani, A. K. Perez, C. Lin and G. Caruntu, *Chem. Mater.*, 2010, **22**, 6075.
45 J. A. Lewis, *J. Am. Ceram. Soc.*, 2000, **83**, 2341.
46 D. Yang, M. Krasowska, R. Sedev and J. Ralston, *Phys. Chem. Chem. Phys.*, 2010, **12**, 13724.
47 A. Pettersson, G. Marino, A. Pursiheimo and J. B. Rosenholm, *J. Colloid Interface Sci.*, 2000, **228**, 73.
48 A. L. Patterson, *Phys. Rev.*, 1939, **56**, 978.
49 F. Cheng, Z. Tao, J. Liang and J. Chen, *Chem. Mater.*, 2008, **20**, 667.
50 B. A. Hernandez, K. S. Chang, E. R. Fisher and P. K. Dorhout, *Chem. Mater.*, 2002, **14**, 480.
51 J. Kim, S. A. Yang, Y. C. Choi, J. K. Han, K. O. Jeong, Y. J. Yun, D. J. Kim, S. M. Yang, D. Yoon, H. Cheong, K. S. Chang, T. W. Noh and S. D. Bu, *Nano Lett.*, 2008, **8**, 1813.
52 Q. Kuang, Z. W. Lin, W. Lian, Z. Y. Jiang, Z. X. Xie, R. B. Huang and L. S. Zheng, *J. Solid State Chem.*, 2007, **180**, 1236.
53 J. H. Wang, Y. W. Ma and K. Watanabe, *Chem. Mater.*, 2008, **20**, 20.
54 F. S. Li, L. J. Song, D. Zhou, T. Wang, Y. Wang and H. B. Wang, *J. Mater. Sci.*, 2007, **42**, 7214.
55 T. Wang, Y. Wang, F. S. Li, C. T. Xu and D. Zhou, *J. Phys.: Condens. Matter*, 2006, **18**, 10545.


Published on 04 April 2011 on http://pubs.rsc.org | doi:10.1039/C0JM04441E
Downloaded by UNIVERSITY OF NEW ORLEANS on 05 March 2013